



# Fast and efficient nanoparticle trapping using plasmonic connected nanoring apertures

Author	Theodoros D Bouloumis, Domna G Kotsifaki, Xue Han, Sile Nic Chormaic, Viet Giang Truong
journal or publication title	Nanotechnology
volume	32
number	2
page range	025507
year	2020-10-20
Publisher	IOP Publishing Ltd.
Rights	(C) 2020 The Author(s).
Author's flag	publisher
URL	<a href="http://id.nii.ac.jp/1394/00001656/">http://id.nii.ac.jp/1394/00001656/</a>

doi: [info:doi/10.1088/1361-6528/abbca9](https://doi.org/10.1088/1361-6528/abbca9)

PAPER • OPEN ACCESS

## Fast and efficient nanoparticle trapping using plasmonic connected nanoring apertures

To cite this article: Theodoros D Bouloumis *et al* 2021 *Nanotechnology* **32** 025507

View the [article online](#) for updates and enhancements.



**IOP | ebooks™**

Bringing together innovative digital publishing with leading authors from the global scientific community.

Start exploring the collection—download the first chapter of every title for free.

# Fast and efficient nanoparticle trapping using plasmonic connected nanoring apertures

Theodoros D Bouloumis<sup>1</sup> , Domna G Kotsifaki<sup>1</sup> , Xue Han<sup>2</sup> ,  
Síle Nic Chormaic<sup>1</sup>  and Viet Giang Truong<sup>1</sup> 

<sup>1</sup>Light-Matter Interactions for Quantum Technologies Unit, Okinawa Institute of Science and Technology Graduate University, Onna-San, Okinawa, Japan

<sup>2</sup>School of Optoelectronic Engineering and Instrumentation Science, Dalian University of Technology, Dalian, Liaoning, People's Republic of China

E-mail: [sile.nichormaic@oist.jp](mailto:sile.nichormaic@oist.jp)

Received 21 July 2020, revised 18 September 2020

Accepted for publication 29 September 2020

Published 20 October 2020



CrossMark

## Abstract

The manipulation of microparticles using optical forces has led to many applications in the life and physical sciences. To extend optical trapping towards the nano-regime, in this work we demonstrate trapping of single nanoparticles in arrays of plasmonic coaxial nano-apertures with various inner disk sizes and theoretically estimate the associated forces. A high normalized experimental trap stiffness of  $3.50 \text{ fN nm}^{-1} \text{ mW}^{-1} \mu\text{m}^{-2}$  for 20 nm polystyrene particles is observed for an optimum design of 149 nm for the nanodisk diameter at a trapping wavelength of 980 nm. Theoretical simulations are used to interpret the enhancement of the observed trap stiffness. A quick particle trapping time of less than 8 s is obtained at a concentration of  $14 \times 10^{11} \text{ particles ml}^{-1}$  with low incident laser intensity of  $0.59 \text{ mW } \mu\text{m}^{-2}$ . This good trapping performance with fast delivery of nanoparticles to multiple trapping sites emerges from a combination of the enhanced electromagnetic near-field and spatial temperature increase. This work has applications in nanoparticle delivery and trapping with high accuracy, and bridges the gap between optical manipulation and nanofluidics.

Keywords: nanoparticles, nanostructured array, optical forces, plasmonic optical tweezers, coaxial aperture, trap stiffness, trapping time


(Some figures may appear in colour only in the online journal)

## 1. Introduction

Optical tweezers are a powerful tool to trap and manipulate particles whose size ranges from a few hundred nanometers to tens of micrometers [1]. Despite numerous applications, optical trapping of particles with sizes smaller than the wavelength of light remains a considerable challenge due to the diffraction limit, which hinders the trapping process.

Pushing optical trapping into the subwavelength regime is achieved with plasmonic optical tweezers (POTs) [2–6], ushering in a new era of experiments at the single nanoparticle level. POTs rely on subwavelength confinement of the trapping laser beam into highly intense hotspots. Complex metallic nanostructures are used to create such plasmonic hotspots, which strongly enhance the amplitude of the electric field of the incident trapping laser. This increased electric field compensates for the low polarisability of nanosized particles, resulting in narrower and deeper trapping potential wells compared to conventional optical tweezers.

A critical issue for trapping individual nanoparticles in an aqueous environment is how to manipulate them towards a

 Original content from this work may be used under the terms of the [Creative Commons Attribution 4.0 licence](https://creativecommons.org/licenses/by/4.0/). Any further distribution of this work must maintain attribution to the author(s) and the title of the work, journal citation and DOI.

given localized near-field hotspot, where they can be trapped by optical gradient forces [7, 8]. To address this problem, there are different approaches that primarily enable transport and trapping with plasmonic nano-antennas. Among these techniques, periodic arrays of closely spaced nano-antennas, e.g. arrays of metallic nanodisks [9], bowtie nanocavities [10], gold nanopyramidal-dimers [11], etc, have gained considerable interest. In all cases, collective heating, due to nearby hotspots, produces strong fluidic thermal convection and thermophoresis, which exert drag forces on the suspended particles and impact their motion [7, 10]. This intrinsic thermoplasmonic convection is exploited for fluid transport [10–12]; hence, particles can mobilize into the area illuminated by the incident laser with relatively fast fluid motion ( $1 \mu\text{m s}^{-1}$ ) [13]. Nevertheless, this method suffers from the issue of ensembles of particles or agglomeration over the surface of the metallic nanostructured array [10–12], leading to difficulty in addressing single nanoparticle trapping at a given hotspot.

A different approach for trapping single nano-objects involves the illumination of a single plasmonic nanostructured element, i.e. a single or a double-nanohole on a metallic thin film [14, 15]. In this approach, collective heating is absent and the intrinsic thermoplasmonic convection is very weak, i.e. the convection fluid velocity is less than  $10 \text{ nm s}^{-1}$  [15–17]. Therefore, the trapping process is mainly due to the optical gradient force [18, 19]. Experimentally, the trapping of individual nano-objects (smaller than 10nm in diameter) has been demonstrated at relatively low laser intensities of less than  $1 \text{ mW } \mu\text{m}^{-2}$  [14, 15, 18, 20, 21]. In spite intense interest in the trapping of nanoparticles with low light trapping powers, the movement of the suspended particles relies on Brownian motion and is diffusion-limited [17, 18]. Consequently, only particles in close proximity to the plasmonic nanostructure can be effectively trapped, placing a limit on working with low concentration and high speed particle trapping applications [7, 8]. Another approach to transport particles to a specific plasmonic hotspot is by integrating an AC electric field with plasmonic nano-antenna resonators [7]. However, the electro-thermo-plasmonic flow associated with the small temperature gradient opto-thermally generated at a single plasmonic nano-antenna is too weak for effective particle delivery.

Recently, we proposed and demonstrated arrays of nanoring apertures for multiple particle trapping for long trapping periods using low incident laser powers [22–24]. The trapping site density was increased by introducing 50 nm connecting gaps between neighboring nanoring apertures. Using such a device, we trapped and transported polystyrene (PS) particles of  $0.5 \mu\text{m}$  and  $1 \mu\text{m}$  diameter across the device's surface with a trapping laser intensity of  $1.5 \text{ mW } \mu\text{m}^{-2}$  [23]. To trap single nanoparticles (30 nm, dielectric), a modified double nanohole array was illuminated by light with an intensity of  $0.51 \text{ mW } \mu\text{m}^{-2}$  for on-resonance conditions [24]. Most recently, we fabricated arrays of asymmetric, Fano resonance, split nano-apertures for trapping single 20nm PS particles on a 50 nm gold thin film. A very large normalized trap stiffness of  $8.65 \text{ fN nm}^{-1} \text{ mW}^{-1}$  was achieved [25]. An

important feature in using these double nanohole/Fano resonance POT aperture arrays is that one can trap individual nanoparticles at low incident powers. Not only does our POT system largely improve the trap stiffness, it also reduces diffusion-limited trapping. The average diffusion time to mobilize particles towards the illuminated trapping area reduces from 15 to 20 min for a typical single nano-element POT [15] to approximately 60 s for the POT aperture array [24, 25] at a similar incident laser intensity ( $\sim 1 \text{ mW } \mu\text{m}^{-2}$ ) and particle concentration of  $14 \times 10^{11} \text{ particles ml}^{-1}$  [15, 26] in water solution.

In this paper, we theoretically calculate the optical forces and trap stiffnesses for a POTs and experimentally demonstrate an efficient optical tweezers for 20 nm PS particle trapping. We use a similar POT design as before [23]. The designed structure was used to trap 20 nm polystyrene particles at the nanoslot region instead of trapping 0.5 and  $1 \mu\text{m}$  (in sizes) polystyrene particles over the sample's surface. Benefiting from the enhancement of the absorption cross-section at resonant conditions by introducing coaxial inner disks, the trap stiffness increases by a factor of about three times compared to that for our previous nanohole array [24]. The average time until the first observed trapping event is reduced from 20 s (nanohole structure) to 8 s (nanohole plus disk structure) for a low laser intensity of  $0.59 \text{ mW } \mu\text{m}^{-2}$  and a concentration of  $14 \times 10^{11} \text{ particles ml}^{-1}$ . This POT design has the potential to not only precisely deliver microparticles (or analytes) to various locations on a chip environment [24], but also can be used to trap small objects of approximately 20 nm with high accuracy. This opens the way for the development of a non-destructive and highly sensitive tool for the delivery, detection and trapping of single molecules at a specific trapping position.

## 2. Results and discussion

### 2.1. Absorption resonance and optical force calculation

The three-dimensional (3D) nano-aperture platform is illustrated in figure 1(a). Nanoring air apertures are engraved on a 50 nm thick gold (Au) metal layer deposited on a quartz substrate. Narrow nanoslot regions are formed by inserting connecting nanogaps between the ring apertures. The plasmonic substrate consists of a 12 (x-direction)  $\times$  13 (y-direction) array of individual nanoring apertures that are milled using the focussed ion beam technique in a 50 nm thick Au film. Scanning electron microscope images are used to obtain the dimensions of the nano-apertures, as shown in figure 1(b). The outer diameter of the nanoring is  $d_{\text{out}} = 285.14 \pm 3.73 \text{ nm}$ , the period of the array,  $\Lambda = 361.71 \pm 1.29 \text{ nm}$ , the width of the connecting nanoslots (gap size between the two tips)  $w_{\text{slot}} = 28.08 \pm 6.04 \text{ nm}$ , and the inner diameter of the coaxial inner disks,  $d_{\text{in}}$ , are 0 nm,  $149.59 \pm 2.08 \text{ nm}$ ,  $173.51 \pm 2.18 \text{ nm}$ , and  $195.28 \pm 1.71 \text{ nm}$ .

The incident light is polarized along the y-axis to highly confine the electric field ( $E$ -field) at the nanoslot area. We use the finite element method with the COMSOL Multiphysics software package to simulate the  $E$ -field distribution and the

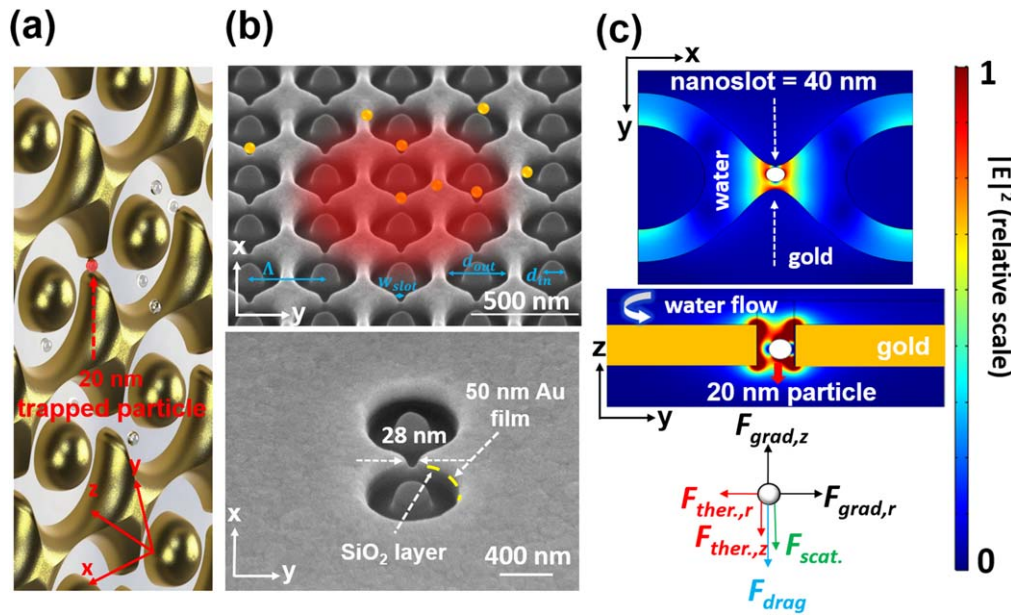


**Figure 1.** (a) Schematic of an array of nanoring nano-apertures. (b) Scanning electron microscope (SEM) images of an array of fabricated nano-apertures in which the sample is tilted by  $52^\circ$  from the surface normal. The outer ring diameter,  $d_{out}$ , of all plasmonic devices is kept constant, while the connecting slit,  $w_{slot}$ , has a width of 28 nm. The concept of nanoparticle trapping is also illustrated. (c) Electric field distribution profiles of a single element of the array in the  $xy$ - and  $yz$ -planes. The trapping spots appear to be at the walls of the nanoslot with 40 nm width and 80 nm depth. The major forces acting on the trapped nanoparticle are illustrated, with  $F_{grad}$ ,  $F_{scat.}$ ,  $F_{drag}$  and  $F_{ther.}$  being the gradient force, the scattering force, the drag force and the thermophoresis, respectively.

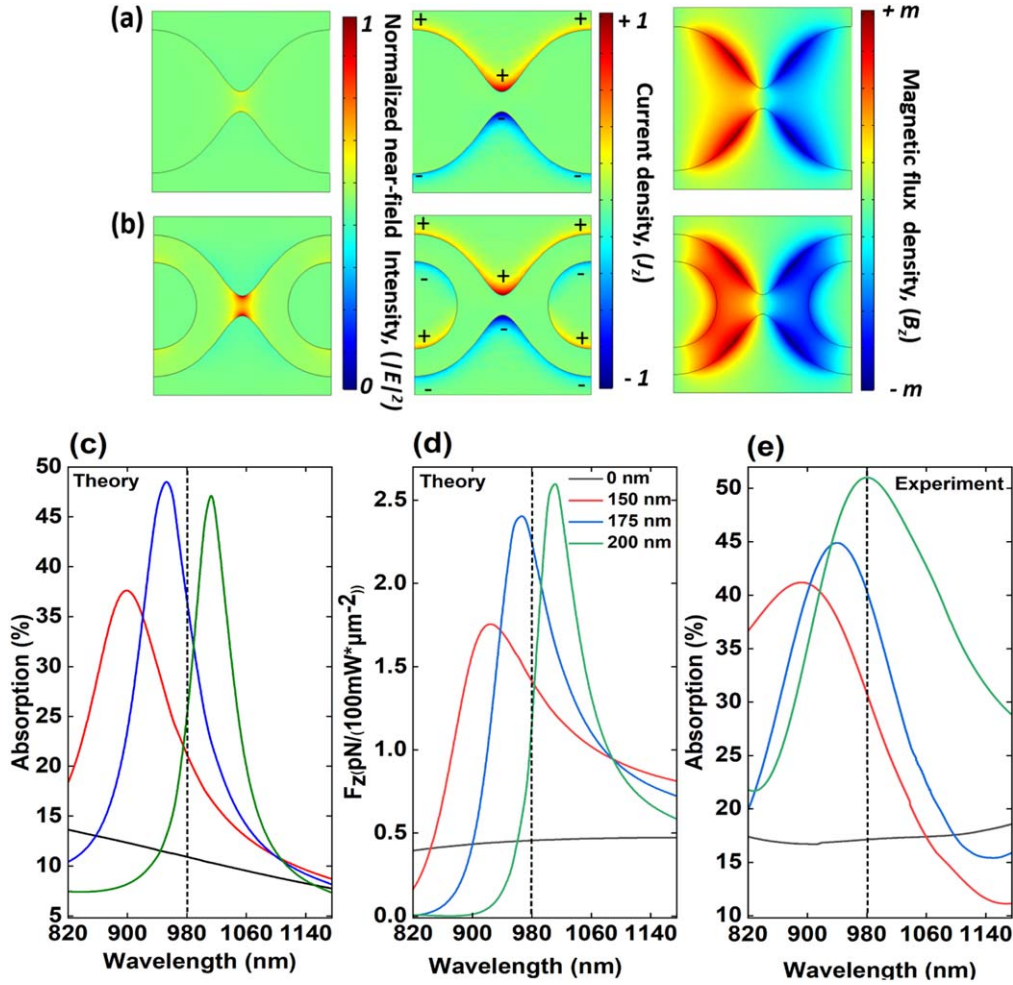
absorption spectra of the devices. We apply the time-averaged Maxwell's stress tensor [27] method to calculate the optical gradient force acting on a 20 nm PS particle. The geometric parameters used in numerical simulations are:  $d_{out} = 285$  nm,  $\Lambda = 360$  nm,  $w_{slot} = 40$  nm, and  $d_{in} = 0, 150, 175, 200$  nm. We assume that the 20 nm particles are trapped 5 nm away from the surface of the device. To obtain good resolution for the mesh size at the particle's surface, we choose the nanoslot width to be 20 nm larger than the particle diameter. The Maxwell's stress tensor is applied on a surrounding shell 2 nm away from the particle's surface. Figure 1(c) shows an example of numerical simulations of the  $E$ -field distribution for the  $xy$ - and  $yz$ -planes with a particle positioned at  $x = 0$  nm and  $z = 20$  nm (the equilibrium position).

Figure 2 shows the normalized near-field intensity, the current density,  $J_z$ , and the magnetic flux density,  $B_z$ , of the  $z$ -component at 980 nm, for arrays (a) without and (b) with an inner disk of diameter 175 nm. Strong near-field enhancement is observed for the array with the inner disk compared to the nanohole configuration. The electromagnetic field oscillates at the frequency of the incident light. The electric field component of this incident light excited the local dipole-like oscillation at the nanotip regions. The magnetic field component oscillates out of phase at the resonant frequency and spreads over into the open area of the nanodisk and outer hole cavity. This bowtie-like open gap area of the ring and disk nanostructure can be considered as a combination of an oscillating electric dipole and a magnetic dipole around the nanotips of the slot area and results in a sharp resonant peak in the absorption spectrum.

Absorption peak spectra are used as indicators of the resonance positions for the various structures used in the study. Figure 2(c) shows the theoretical absorption spectra for all the structures with varying inner disk diameters,  $d_{in} = 0$ –200 nm, in water solution. Note that, with increased inner disk size, the absorption peak is red-shifted, which allows us to tune the required excitation laser towards the experimental wavelength of 980 nm. The red-shifted behavior of the absorption peak is due to the increase of charges accumulating around the edge regions of the inner disk and the outer hole. This redistribution of charges around the outer hole edge leads to a strong increase of the local charge stored on the nanotips of the slot area. Of the four devices, the 175 nm inner disk design shows the highest theoretical absorption peak at 980 nm (vertical dotted line in figure 2(c)). In figure 2(d), we plot the theoretical optical trapping force along the  $z$ -axis (light propagation direction), acting on a 20 nm PS nanoparticle at  $(x, y, z) = (0, 0, -4)$  nm position, where the localized field intensity is highest, as a function of the excitation laser wavelength. For excitation at 980 nm, the 175 nm design exerts the strongest theoretical optical force, of about  $2.24$  pN/(100 mW  $\mu\text{m}^{-2}$ ), on the nanoparticle. We see that the theoretical absorption spectra and  $z$ -component of the optical trapping force show similar curve trends. However, the theoretical trapping force peak positions show a slight red-shift towards the 980 nm excitation wavelength compared to the theoretical absorption resonance peaks. It is worth noting that the optical force is relatively constant for the 0 nm design (no inner disk) within this wavelength range.

To perform the experimental measurement of absorption, a microspectrophotometer (MCRAIC 20/30 PV) is used to





**Figure 2.** Normalized near-field intensity (left column), current density (middle column),  $J_z$  and magnetic flux density (right column),  $B_z$ , of the  $z$ -component for a wavelength  $\lambda = 980$  nm for arrays (a) with no inner disks and (b) with 175 nm inner disks. The electric and magnetic fields are localized around the nanotips of the nano-slot area. (c) Theoretical absorption spectra for the nano-aperture designs with inner disk diameters 0, 150, 175, and 200 nm. (d) Simulated optical force,  $F_z$ , along the light propagation direction, acting on a 20 nm diameter PS particle in water. The optical force is normalized to 100 mW  $\mu\text{m}^{-2}$  incident light intensity. (e) The absorption spectra of an array of 42 units in deionized water with the polarization of the microspectrophotometer light source along the  $y$ -direction. The dotted vertical line indicates the wavelength of the laser in trapping experiments.

measure the reflection,  $R$ , and transmission,  $T$ , spectra of the plasmonic devices in deionized water. The absorption,  $A$ , is determined from the following:  $A(\%) = 100(\%) - T(\%) - R(\%)$  and indicates the resonance peak position for the nanoring array structures, see figure 2(e). We notice that the wavelength is blue-shifted by approximately 20 nm compared to the theoretical curves (figure 2(c)). We assume that this discrepancy arises from imperfections during the fabrication process leading to rounded edges in the structure's features, in contrast to sharp edges in simulations. The experimental trapping laser beam at 980 nm is at a value far from these peaks. This allows us to extract information on the enhancement of the absorption spectrum for each plasmonic configuration. The intersection point between the vertical dashed line at  $\lambda = 980$  nm and the absorption spectra indicates an absorption magnitude increase of 17%, 31%, 41% and 51% for the 0 nm, 150 nm, 175 nm and 200 nm plasmonic configuration, respectively.

## 2.2. Optical potential well and trap stiffness

The optical trapping force, its corresponding potential, and trap stiffness for a 20 nm PS particle in the proximity of the 3D plasmonic nanoslot area are numerically calculated using the COMSOL Multiphysics software package. We assume that the particle is in the water domain of the  $xy$ -plane and sweep the particle along the  $z$ -axis (see figure 1(b)). We obtain the potentials by integrating the corresponding forces along the  $z$ -axis. The incident laser intensity is 100 mW  $\mu\text{m}^{-2}$  at 980 nm.

In our model, the plane at  $z = 0$  nm is the boundary between the Au film and the water domain. The thickness of the Au film is 50 nm, thus for positions in the range of 0–50 nm along  $z$  the particle is within the water-filled nanoslot region of the Au film. The optical force has a positive sign when the particle is attracted towards the SiO<sub>2</sub> domain and a negative sign indicates a repulsive force in the opposite direction. Moreover, the equilibrium position for trapped

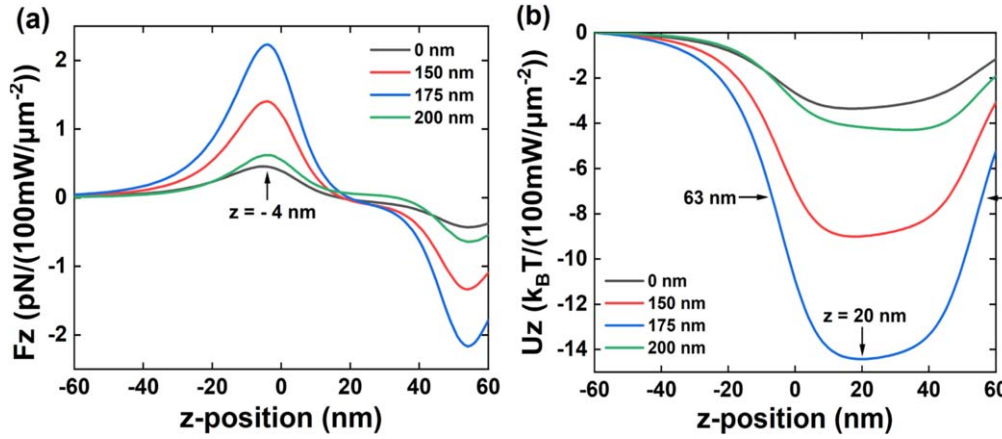


**Figure 3.** (a) Optical forces along the  $z$ -axis for 980 nm illumination. The maximum optical force is at  $z = -4$  nm for all designs. (b) Corresponding potentials of the optical forces in (a). The depths of the wells have a similar behavior as the optical forces, with the 175 nm inner disk diameter design exhibiting the deepest and broadest well, with a full-width-at-half-maximum of 63 nm. The equilibrium position is around  $z = 20$  nm.

particles is located at  $z = 20$  nm, i.e. inside the nanoslot area, for all designs. Figures 3(a) and (b) show the calculated optical forces and their corresponding potentials along the  $z$ -axis for four different nanodisk structures.

We also calculate the trapping potentials along the  $x$ - and  $y$ -axis for the 175 nm inner disk diameter and at the  $z = -4$  nm plane, where the strongest optical force is observed (data not shown). We obtain a full-width-at-half-maximum (FWHM) of the trapping wells in the  $x$ -direction to be 44 nm and 14.4 nm in the  $y$ -direction, which is almost four times narrower due to stronger trapping. This arises since the  $E$ -field is highly confined (i.e. stronger gradient) at the nanoslot along the  $y$ -direction.

Finally, the trap stiffness,  $\kappa$ , is calculated for the 175 nm inner disk design, along all three axes. We use the harmonic oscillator equation,  $F = \kappa\Delta r$ , where  $F$  is the maximum optical force acting on the nanoparticle for each axis and  $\Delta r$  is the FWHM/2. We also normalize all values to  $1 \text{ mW } \mu\text{m}^{-2}$  incident light intensity. We determine that  $\kappa_x = 0.55 \text{ fN nm}^{-1}$ ,  $\kappa_y = 3.72 \text{ fN nm}^{-1}$ , and  $\kappa_z = 0.71 \text{ fN nm}^{-1}$ . The total trap stiffness is  $\kappa_{\text{tot}} = \sqrt{\kappa_x^2 + \kappa_y^2 + \kappa_z^2} = 3.82 \text{ fN nm}^{-1}$ .

The structure with the 175 nm inner disk diameter has the highest theoretical absorbance efficiency, provides the maximum theoretical optical force on a 20 nm particle, and creates the deepest trapping potential of  $-14.42k_B T/(100 \text{ mW } \mu\text{m}^{-2})$ . As mentioned previously, there is a 20 nm blue-shift of the experimental absorption peak positions compared to theoretical calculations. We observe that the fabricated 200 nm design nanodisk shows the strongest experimental absorbance at 980 nm (vertical dashed line in figure 3(e)). Based on theoretical interpretations, we conclude here that the 175 nm nanodisk structure should provide the strongest experimental optical trapping force on a 20 nm PS particle in water solution for the excitation wavelength of 980 nm.

### 2.3. Trap performance evaluation

The experimental approach is described in our previous work [25]. In brief, for nanoparticle trapping experiments, a tunable,

continuous-wave Ti:Sapphire laser (MBR110 Coherent) is used at 980 nm. The laser spot diameter at the sample plane is around  $2 \mu\text{m}$ . The number of nanorings that can be excited on the plasmonic substrates is 25, based on the size of the incident trapping laser spot. A high numerical aperture (N.A. = 1.3) oil immersion objective lens (OLYMPUS UPlanFL N 100 $\times$ ) is used to focus the trapping beam onto the plasmonic substrate. We control the incident power of the trapping beam, which is limited to a maximum of 7.7 mW, at the sample plane, while the polarization of the trapping laser is along the  $y$ -direction (see figure 1). A trapping event is detected by collecting the transmitted laser light through a 50 $\times$  objective lens (Nikon CF Plan) and sending it to an avalanche photodiode (APD430A/M, Thorlabs). The APD signal is recorded using a data acquisition board at a frequency of 100 kHz with a LabVIEW program. When a 20 nm particle is trapped in one connecting nanoslot, a sharp increase in transmission is observed. The transmission level returns to its initial value when there is no particle at the trapping point. The plasmonic substrate is attached to a cover glass with adhesive microscope spacers, forming a microwell. The microwell contains  $8 \mu\text{l}$  of PS nanoparticles with a mean diameter of 20 nm (Thermo Fisher Scientific, F8786) in heavy water with a concentration of  $14 \times 10^{11} \text{ particles ml}^{-1}$ . A small amount of surfactant (Detergent Tween 20 with 0.1% volume concentration) is used to minimize particle aggregation. The microwell is mounted and fixed on top of a piezoelectric translation stage.

Figure 4(a) shows the measured trap stiffnesses,  $\kappa_{\text{exp}}$ , for four different inner disk diameters,  $d_{\text{in}}$ , as a function of the incident laser intensity. We use the transient time method as discussed elsewhere [24–26]. We also consider Faxén's correction to introduce a factored drag force that arises due to the surface roughness of the nanoring structure wall, as previously reported for nanoparticle trapping [24–26]. The trapping laser intensity ranges from 0.48 to  $1.03 \text{ mW } \mu\text{m}^{-2}$ . The experimental trap stiffness is the average over three multiple runs for each laser intensity. It should be noted that a trapping laser intensity of less than  $1.03 \text{ mW } \mu\text{m}^{-2}$  at  $\lambda = 980 \text{ nm}$  (off-resonant condition) must be used to prevent

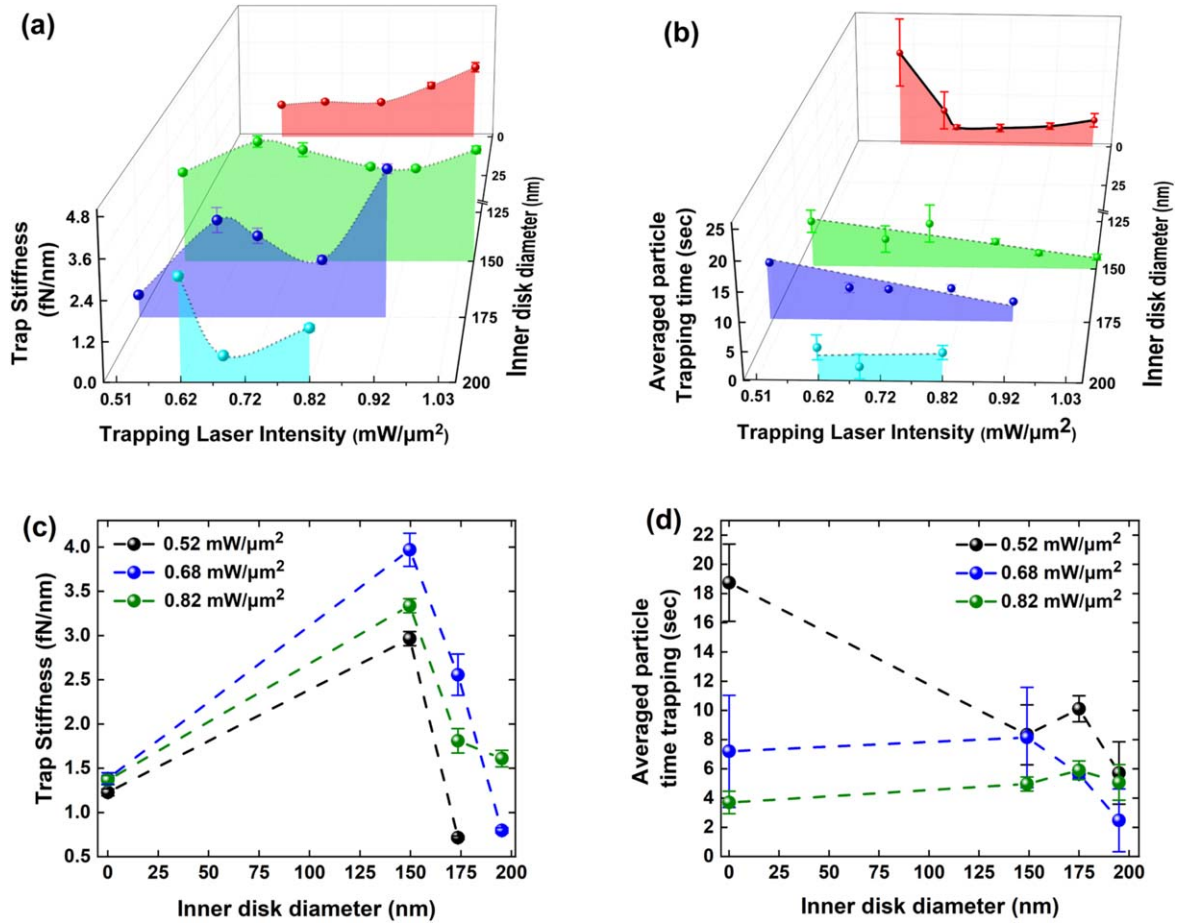


**Figure 4.** (a) Trap stiffness for a 20 nm PS particle as a function of incident laser intensity and inner disk diameter. The dotted lines serve as visual aids. (b) Average particle trapping time as a function of trapping laser intensity and inner disk diameter. The black solid line for 0 nm inner disk diameter serves as a visual aid while the dashed lines are linear fits to the experimental results. Each color represents a different disk diameter. (c) Trap stiffness and (d) average time to trap a particle as a function of inner disk diameter for 0.52, 0.68, and 0.82  $\text{mW } \mu\text{m}^{-2}$  incident laser intensities. The points plotted are averaged values over three trapping events for different laser intensities (different colors), along with their standard deviations.

any cluster formation [10] and to achieve stable single-nanoparticle trapping.

As expected, we observe an increase to the measured trap stiffnesses for larger inner disk structures compared to the no-disk configuration. When there is no disk (red curve in figure 4(a)), the trap stiffness is relatively constant for trapping laser intensities below  $0.75 \text{ mW } \mu\text{m}^{-2}$  and increases linearly for higher trapping laser intensities. This behavior changes for the nanoring array with  $d_{\text{in}} = 149 \text{ nm}$  (green curve in figure 4(a)), where the trap stiffness does not vary significantly as the incident laser intensity increases to  $1.03 \text{ mW } \mu\text{m}^{-2}$ . Surprisingly, as the inner disk diameter increases, larger fluctuations of the trap stiffness are evident and the expected linear behavior is not observed. A maximum trap stiffness is achieved for the 149 nm inner disk configuration (purple curve in figure 4(a)). We also note that the 195 nm inner disk diameter device (blue curve in figure 4(a)), which is expected to produce the highest optical trapping force, does not provide the maximum trap stiffness for both low,  $0.52 \text{ mW } \mu\text{m}^{-2}$ , and high,  $0.82 \text{ mW } \mu\text{m}^{-2}$ , laser intensities, (figure 4(c)). Instead, the trap stiffness for larger inner disk diameters of 173 and 195 nm decreases compared to the 149 nm inner disk structure. Assuming that, as the inner

disk diameter increases, thermal energy dissipation via the Joule effect increases upon resonant excitation, an increase of the spatial temperature distribution would result. This is due to collective heating of several hotspots in the illumination area of the nano-aperture array. This photo-induced plasmonic heating produces a temperature gradient across the device, resulting in the creation of a strong thermal fluidic flow, which could influence the trap stiffness values. Furthermore, the discrepancy between the theoretical optical force calculation and experimental stiffness observation for different nanodisk sizes could be due to an increase in the Brownian motion. Nevertheless, we did not observe particles escaping from the trap during the experiments. Therefore, we conclude that the increase to the Brownian motion is not sufficient to enable the nanoparticle to escape from the potential well for the specific laser intensity ranging from  $0.51$  to  $1.03 \text{ mW } \mu\text{m}^{-2}$ .

The maximum  $\kappa_{\text{exp}} = 3.50 \pm 0.17 \text{ fN nm}^{-1}$  is obtained for the nanoring array with 149 nm inner disk diameter. The stiffness enhancement factor is approximately 2.9, 1.8, and 0.6 times for the nanoring arrays of  $d_{\text{in}} = 149 \text{ nm}$ ,  $d_{\text{in}} = 173 \text{ nm}$ , and  $d_{\text{in}} = 195 \text{ nm}$ , respectively, when compared to the standard,  $d_{\text{in}} = 0 \text{ nm}$ , nanohole array configuration for an incident laser



intensity of  $1.0 \text{ mW } \mu\text{m}^{-2}$  at 980 nm. The high trap stiffness for the 149 nm inner disk diameter indicates the ability of this device to perform stable trapping and to hold nanoparticles at specific positions for long periods of time, thereby providing opportunities for effective low-power nanomanufacturing of nanoscale objects.

Figure 4(b) shows the average time taken to trap a single 20 nm particle as a function of the trapping laser intensity for different inner disk diameters. The trapping time is defined as the time from when the trapping laser is turned on ( $t = 0$ ) to the transmission signal's first observed discrete step, indicating the first particle trapping event. The experimental trapping time is taken from the average values observed over three multiple runs. The error bars represent the standard deviation of the average trapping time measurements. We also assume that, as the trapping laser intensity increases, the spatial temperature distribution increases, producing buoyancy-driven natural convection due to the fluid's density gradient. This leads to an increase in the probability of trapping a nanoparticle in the flow, delivering it to the illuminated area, thus reducing the average particle trapping time. We also note that, for low laser intensities, the array of nano-apertures (0 nm inner disk) provides the longest particle diffusion times (figure 4(d)). Specifically, for  $0.55 \text{ mW } \mu\text{m}^{-2}$  laser intensity, the trapping time for the 0 nm and 149 nm inner disk designs is 18.7 s and 8.3 s, respectively. A linear behavior of the average particle trapping time as a function of laser intensity is observed for configurations with 149 and 173 nm inner disk diameters with slopes of  $1.72 \pm 0.35 \text{ s mW}^{-1} \mu\text{m}^{-2}$  and  $2.53 \pm 0.65 \text{ s mW}^{-1} \mu\text{m}^{-2}$ , respectively. Figure 4(d) shows that the average particle trapping time approaches a minimum value at around 4 s for all nanodisk designs when higher laser intensities up to  $0.82 \text{ mW } \mu\text{m}^{-2}$  are used.

### 3. Conclusion

Heating in plasmonic tweezers has previously been treated as an obstacle to stable trapping of particles. In 2010, Ploschner *et al* performed a computational study of trapping with a plasmonic nano-antenna and suggested that the particle positioning may not be due to optical forces alone [28]. The discrepancies we observe in the values of trap stiffness determined from theory based on optical force calculations and experimental observations indicate that thermophoresis may play a significant role in the trapping process for larger inner disks thereby creating an additional force on the particle due to Stokes' drag. To further understand the origin of this mechanism, a 3D theoretical heating model of plasmonic arrays is required to explore in depth the contribution of thermal convection flows to the trapping performance. A detailed study of particles (e.g. biomolecules, dielectric, or metallic nanoparticles with varying particle concentrations and sizes) will provide insights into the thermally assisted trapping process. Besides these parameters, other benchmarks, such as interactions between particles and the surface, should be addressed for a complete understanding of the experiments. This is beyond the scope of the current work.

In 2014, Roxworthy *et al* showed that an array of plasmonic nano-antennas coupled to an optically absorptive

indium-tin-oxide (ITO) substrate can generate micrometer per second fluid convection [13]. In their system, heating creates a fluid motion capable of rapid particle transport. Here, we replace the absorbing ITO thin film substrate with an array of plasmonic nano-apertures, engraved directly onto a 50 nm metallic Au film. The Au metal film itself facilitates the thermal energy distribution of the Au substrate and the surrounding fluid; hence, heat transfer can occur over large effective areas of the illuminated aperture array. Collective heating of many hotspots achieves better heating efficiency at relatively low laser power excitation compared to a single nano-element trapping configuration. This, in turn, produces buoyancy-driven natural convection currents and can rapidly transport the nanoparticles towards hotspots where they will be trapped in a short time interval. Our approach provides an alternative avenue towards rapid particle delivery and strong single nanoparticle trapping, both of which could play important roles in molecular analysis.

### Acknowledgments

The authors would like to thank M Ozer and S P Mekhail for technical assistance, M Sergides for initial contributions to the experimental work, and OIST editing section for reviewing the manuscript.

### Funding

This work was partly funded by the Okinawa Institute of Science and Technology Graduate University, Onna-San, Okinawa, Japan. DGK acknowledges support from JSPS Grant-in-Aid for Scientific Research (C) Grant Number GD1675001. TDB acknowledges support from the Japan Student Services Organization (JASSO) for the Monbukagakusho (MEXT) Honors Scholarship (2019-2020).

### ORCID iDs

Theodoros D Bouloumis  <https://orcid.org/0000-0002-5264-7338>

Domna G Kotsifaki  <https://orcid.org/0000-0002-2023-8345>

Xue Han  <https://orcid.org/0000-0001-9525-1176>

Síle Nic Chormaic  <https://orcid.org/0000-0003-4276-2014>

Viet Giang Truong  <https://orcid.org/0000-0003-3589-7850>

### References

- [1] Ashkin A 1997 Optical trapping and manipulation of neutral particles using lasers *Proc. Natl Acad. Sci.* **94** 4853–60
- [2] Novotny L, Bian R X and Xie X S 1997 Theory of nanometric optical tweezers *Phys. Rev. Lett.* **79** 645–8
- [3] Daly M, Sergides M and Nic Chormaic S 2015 Optical trapping and manipulation of micrometer and submicrometer particles *Laser Photonics Rev.* **9** 309–29

- [4] Kotsifaki D G and Nic Chormaic S 2019 Plasmonic optical tweezers based on nanostructures: fundamentals, advances and prospects *Nanophotonics* **8** 1227–45
- [5] Bouloumis T D and Nic Chormaic S 2020 From far-field to near-field micro- and nanoparticle optical trapping *Appl. Sci.* **10** 1375
- [6] Marago O M, Jones P H, Gucciardi P G, Volpe G and Ferrari A C 2013 Optical trapping and manipulation of nanostructures *Nat. Nanotechnol.* **8** 807–19
- [7] Ndukaife J C, Kildishev A V, Nnanna A G A, Shalaev V M, Wereley S T and Boltasseva A 2015 Long-range and rapid transport of individual nano-objects by a hybrid electrothermoplasmonic nanotweezer *Nat. Nanotechnol.* **11** 53–9
- [8] Kotnala A, Kollipara P S, Li J and Zheng Y 2020 Overcoming diffusion-limited trapping in nanoaperture tweezers using opto-thermal-induced flow *Nano Lett.* **20** 768–79
- [9] Chen K-Y, Lee A-T, Hung C-C, Huang J-S and Yang Y-T 2013 Transport and trapping in two-dimensional nanoscale plasmonic optical lattice *Nano Lett.* **13** 4118–22
- [10] Roxworthy B J, Ko K D, Kumar A, Fung K H, Chow E K C, Liu G L, Fang N X and Toussaint K C 2012 Application of plasmonic bowtie nanoantenna arrays for optical trapping, stacking, and sorting *Nano Lett.* **12** 796–801
- [11] Shoji T, Shibata M, Kitamura N, Nagasawa F, Takase M, Murakoshi K, Nobuhiro A, Mizumoto Y, Ishihara H and Tsuboi Y 2013 Reversible photoinduced formation and manipulation of a two-dimensional closely packed assembly of polystyrene nanospheres on a metallic nanostructure *J. Phys. Chem. C* **117** 2500–6
- [12] Baffou G, Berto P, Ureña E B, Quidant R, Monneret S, Polleux J and Rigneault H 2013 Photoinduced heating of nanoparticle arrays *ACS Nano* **7** 6478–88
- [13] Roxworthy B J, Bhuiya A M, Vanka S P and Toussaint K C 2014 Understanding and controlling plasmon-induced convection *Nat. Commun.* **5** 3173
- [14] Pang Y and Gordon R 2011 Optical trapping of 12 nm dielectric spheres using double-nanoholes in a gold film *Nano Lett.* **11** 3763–7
- [15] Xu Z, Song W and Crozier K B 2018 Direct particle tracking observation and brownian dynamics simulations of a single nanoparticle optically trapped by a plasmonic nanoaperture *ACS Photonics* **5** 2850–9
- [16] Donner J S, Baffou G, McCloskey D and Quidant R 2011 Plasmon-assisted optofluidics *ACS Nano* **5** 5457–62
- [17] Jiang Q, Rogez B, Claude J-B, Baffou G and Wenger J 2019 Temperature measurement in plasmonic nanoapertures used for optical trapping *ACS Photonics* **6** 1763–73
- [18] Wang K, Schonbrun E, Steinvurzel P and Crozier K B 2011 Trapping and rotating nanoparticles using a plasmonic nanotweezer with an integrated heat sink *Nat. Commun.* **2** 469
- [19] Tanaka Y, Kaneda S and Sasaki K 2013 Nanostructured potential of optical trapping using a plasmonic nanoblock pair *Nano Lett.* **13** 2146–50
- [20] Verschuere D, Shi X and Dekker C 2019 Nano-optical tweezing of single proteins in plasmonic nanopores *Small Methods* **3** 1800465
- [21] Pang Y and Gordon R 2012 Optical trapping of a single protein *Nano Lett.* **12** 402–6
- [22] Sergides M, Truong V G and Nic Chormaic S 2016 Highly tunable plasmonic nanoring arrays for nanoparticle manipulation and detection *Nanotechnology* **27** 365301
- [23] Han X, Truong V G and Nic Chormaic S 2018 Efficient microparticle trapping with plasmonic annular apertures arrays *Nano Futures* **2** 035007
- [24] Han X, Truong V G, Thomas P S and Nic Chormaic S 2018 Sequential trapping of single nanoparticles using a gold plasmonic nanohole array *Photonics Res.* **6** 981–6
- [25] Kotsifaki D G, Truong V G and Nic Chormaic S 2020 Fano-resonant, asymmetric, metamaterial-assisted tweezers for single nanoparticle trapping *Nano Lett.* **20** 3388–95
- [26] Kotnala A and Gordon R 2014 Quantification of high-efficiency trapping of nanoparticles in a double nanohole optical tweezer *Nano Lett.* **14** 853–6
- [27] Stratton J A 1941 *Electromagnetic Theory* (New York: McGraw-Hill)
- [28] Ploschner M, Mazilu M, Krauss T F and Dholakia K 2010 Optical forces near a nanoantenna *J. Nanophotonics* **4** 1–13